Mechanism of the structural phase transformations in epitaxial YHx switchable mirrors

Kooi, B. J.; Zoestbergen, E.; de Hosson, J. Th. M.; Kerssemakers, J. W. J.; Dam, B.; Ward, R. C. C.

Published in:
Journal of Applied Physics

DOI:
10.1063/1.1431427

Mechanism of the structural phase transformations in epitaxial YH_x switchable mirrors

B. J. Kooi, E. Zoestbergen, and J. Th. M. De Hosson[a)]
Department of Applied Physics, Materials Science Center and the Netherlands Institute for Metals Research, University of Groningen, Nijenborgh 4, 9747 AG Groningen, The Netherlands

J. W. J. Kerssemakers and B. Dam
Division of Physics and Astronomy, Faculty of Sciences, Vrije Universiteit, De Boelelaan 1081, 1081 HV Amsterdam, The Netherlands

R. C. C. Ward
Oxford Physics, Clarendon Laboratory, Parks Road, Oxford OX1 3PU, United Kingdom

(Received 31 August 2001; accepted for publication 7 November 2001)

The detailed mechanisms of the structural phase transformations that occur in epitaxial Y–hydride switchable mirrors are revealed with high resolution transmission electron microscopy (both cross sectional and plan view). The triangular ridge network that develops in Y prior to the α–β transformation is a result of $\{10\bar{1}2\}$ deformation twinning. The basal plane that is originally parallel to the film/substrate interface is rotated by twinning over 5.6° and transformed into a prismatic plane and similarly the prismatic plane is transformed into a basal plane giving a final crystal reorientation for the ridge of 95.6°. After transformation to β, nearly vertical $\Sigma 3\{111\}$ twin boundaries arise in the ridges. In contrast, horizontal twin boundaries develop in the β domains to prevent macroscopic shape changes. Inbetween the two twin variants within the domains, Shockley partial dislocations are persistently present, which enable efficient reversible β–γ switching of the mirror. © *2002 American Institute of Physics.* [DOI: 10.1063/1.1431427]

I. INTRODUCTION

Phase transitions in rare-earth metal hydrides have attracted considerable attention, from both a scientific and a technological viewpoint. The former is due to the accompanying metal–insulator transitions, whereas the latter is driven by potential applications as switchable mirrors.[1–6] Upon hydrogen loading, an α-Y film first transforms to β-YH_2, after which the reversible transformation between β-YH_2 and γ-$YH_{3-\delta}$ can take place that is at the origin of the switchable mirror effect. Recently, it was shown that upon loading an epitaxially grown thin film of Y on CaF_2 with H, an irreversible triangular pattern of ridges develops on the surface.[7,8] The domains separated by these ridges were shown to switch independently from each other, that is from the dihydride to the trihydride state. This reversible metal–insulator transition involves a large out of plane lattice expansion. The triangular ridge network appeared to act as a microscopic lubricant for the domain switching and as barriers for lateral H diffusion, which is remarkable since hydrogen diffusion is in general fast along structural defects (dislocations and grain boundaries). In contrast to the domains, the ridges switch collectively.

The ridges already start to develop upon initial hydrogen loading, i.e., with the surrounding of the ridges still in the Y state. The triangular network is not a peculiarity of the YH_x/CaF_2 system, but it was also shown to develop upon H loading of the Ho/α-Al_2O_3 and Gd/W epitaxial systems.[9,10] Some suggestions were made for the crystallographic origin of the ridges in these epitaxial films,[8–10] but up to now no convincing explanations and direct observations of their actual evolution of structures are reported. The objective of this article is to reveal the structure of these ridges by transmission electron microscopy (TEM). Furthermore, although the metal–insulator transitions, i.e., the change in electronic structure upon, e.g., the YH_2–YH_3 transition, have been the subject of intensive studies, the actual structural phase transformations that occur in either polycrystalline or epitaxial thin films have not been examined in great detail. Therefore the main objective is to reveal the mechanisms by which the structural phase transformations occur in epitaxial Y films on both CaF_2 and α-Al_2O_3 substrates. Both the initial α-Y to β-YH_2 as well as the reversible β-YH_2 to γ-$YH_{3-\delta}$ transitions are analyzed using both cross-sectional and plan-view TEM. In addition x-ray diffraction (XRD) texture measurements were performed to study the structure of the β-YH_2 and the γ-$YH_{3-\delta}$ epitaxial films. With TEM it is practically impossible to study γ, because thin TEM foils after preparation have a very strong preference to be in the β state.

α-Y has a close-packed hexagonal structure ($P6_3/mmc$) with $a=0.36747$ nm and $c=0.573$ nm (JCPDS 33-1485). The structure of β-YH_2 is face-centered cubic based ($Fm3m$) with $a=0.52077$ nm (JCPDS 12-0388) and of γ-$YH_{3-\delta}$ is hexagonal ($P\bar{3}c1$) with $a=0.6358$ nm and $c=0.662$ nm (JCPDS 12-0385). In order to compare the a axes of α-Y and γ-$YH_{3-\delta}$ the a axis of the latter should be divided by $\sqrt{3}$, which would hold if the hydrogen atoms would occupy the interstitial sites within the Y sublattice of γ

[a)]Author to whom correspondence should be addressed; electronic mail: hossonj@phys.rug.nl

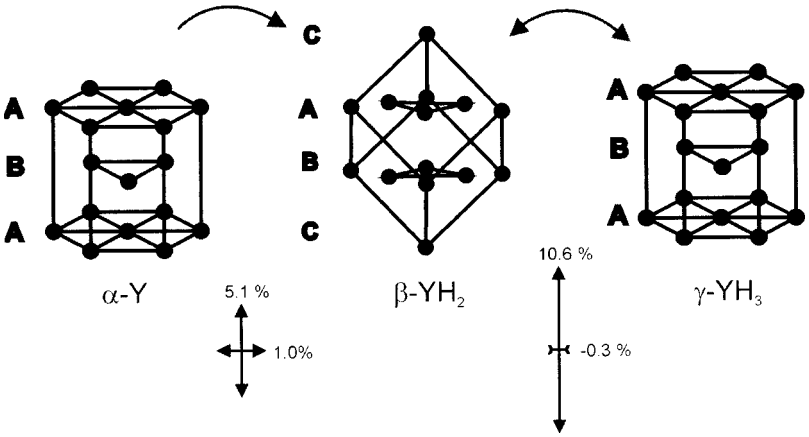

FIG. 1. Schematic representation of the crystal structures with relative orientations and lattice expansions of the phases involved in the domains of epitaxial YH_x switchable mirrors, where α-Y is grown with the basal plane parallel to the substrate surface.

in a disordered instead of an ordered manner. On both CaF_2 and α-Al_2O_3, the α-Y film grows with the *c* axis parallel to the normal of the substrate surfaces. In Fig. 1 the crystal orientations of α, β, and γ observed for the domains of the epitaxial YH_x switchable mirror[7,11] are schematically depicted together with the accompanying in-plane and out-of-plane expansions.

II. EXPERIMENT

Epitaxial YH_x-switchable mirrors are prepared by electron gun evaporation of yttrium on $CaF_2(111)$ substrates at elevated temperatures (300–700 °C) in ultrahigh vacuum (base pressure 10^{-9} mbar).[7] The Y film analyzed in this work is capped with 20 nm CaF_2 and with 20 nm Pd in order to protect the Y from oxidation and to promote H_2 dissociation. The film was exposed to hydrogen in order to form YH_2, but due to the relative thick CaF_2 capping layer H diffusion proceeded through pin holes in this layer. In fact many lateral diffusion experiments[5] were carried out simultaneously. The H loading was interrupted when a part of the Y film had transformed into YH_2. This sample type was then analyzed extensively in plan view with TEM. We were very fortunate that the final TEM sample still contained Y next to YH_2, probably because the Y was protected by the CaF_2 substrate and capping layer most of the time. For both cross-sectional and plan-view TEM another type of sample is used. It consists of a 500 nm Y film epitaxially grown on a 5 nm Nb interlayer on an α-$Al_2O_3(11\bar{2}0)$ substrate with the Balzers UMS630 molecular beam epitaxy facility at Oxford. On top of the Y layer first a 5 nm Nb followed by a 5 nm Pd capping layer is grown. The films on the sapphire substrate are investigated after loading with hydrogen in two different ways. First, an attempt was made to obtain a film that consisted of both Y and YH_2. To this purpose in one sample we interrupted the hydrogen loading during the transformation of Y to YH_2, after ridge formation has clearly been established. Another film was fully loaded to the YH_3 phase after which a natural release of hydrogen to the YH_2 phase was allowed to occur. In TEM both samples turned out to be fully YH_2, although their loading routes were principally different.

Cross-sectional TEM samples were obtained using a standard procedure. Slices with a width of about 1 mm were cut from the sapphire/YH_x samples. Two slices were glued together with the original YH_x films facing each other and separated by the glue (Gatan G-1 epoxy and hardener). The coupled slices were glued in cross-section geometry on a Cu ring (3 mm outer and 2 mm inner diameter). Then the sapphire/YH_x is ground and polished to a thickness of about 15 μm using a tripod. Finally, the polished sample is thinned to electron transparency by two beams of 4 kV Ar^+ ions making angles of 6° with the top and bottom sample surfaces using a Gatan PIPS 691. Plan-view samples of YH_x films on both sapphire and CaF_2 substrates are obtained by first gluing together a piece of the material with the thin-film side on a Cu ring followed by polishing and dimpling procedures of the back side of the substrate until the central thickness is about 20 μm. Finally, the dimpled sample is thinned to electron transparency using 4 kV Ar^+ ion beams making angles of 6° with the back side of the sample. Care was taken (using a covering glass) to avoid contamination on the thin-film side of the sample. Because of the thin capping films on the YH_x film (Nb and Pd on the YH_x film on sapphire and Pd and CaF_2 on the YH_x film on CaF_2) several short ion-milling steps, with intermediate checking in the microscope, are carried out to remove these layers. TEM examinations were performed using a JEOL 4000 EX/II operating at 400 kV (point resolution 0.165 nm).

III. RESULTS

Figure 2 shows a cross-sectional high resolution TEM (HRTEM) image of the interface structure of a hydrogen loaded 500 nm Y film epitaxially grown on a α-$Al_2O_3(11\bar{2}0)$ substrate by means of an intermediate layer of 5 nm Nb. Within the domains one set of close-packed YH_2 {111} planes is parallel to the interface. Details about the exact orientation relation between α-Al_2O_3 with Nb and with Y (and YH_2 and $YH_{3-\delta}$ in the domains) are given in Refs. 9 and 11. Within the YH_2 domains (with a height of 500 nm) a large density of $\Sigma 3\{111\}$ twin boundaries with the boundary plane parallel to the interface plane is observed [see Figs. 3(a)–3(c)]. The average thickness of the twin lamellae in the 500 nm films on sapphire is 48 nm with a standard deviation of 29 nm (36 lamellae measured). Steps (ledges) or step segments (super ledges) are present on the twin boundaries. An example of a super ledge is shown in

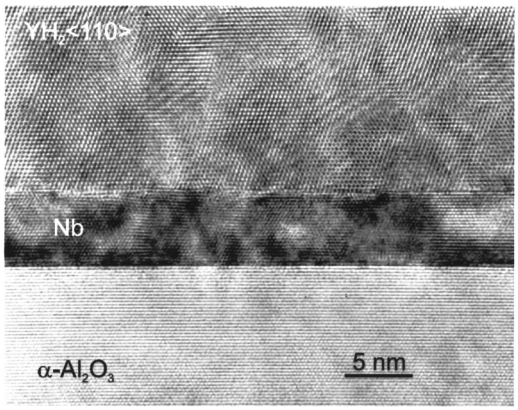

FIG. 2. Cross-sectional HRTEM image showing the interface structure of a 500 nm YH_2 film epitaxially grown on a α-$Al_2O_3(11\bar{2}0)$ substrate by means of an intermediate layer of 5 nm Nb. Within the domains one set of close-packed $YH_2\{111\}$ planes is parallel to the interface plane.

Fig. 3(b). Also twin lamellae as bounded by two $\Sigma 3\{111\}$ boundaries can stop abruptly [see Fig. 3(c)]. At all these locations where the two twin variants meet on the same {111} plane parallel to the Y/Nb/α-Al_2O_3 interface, a Shockley partial dislocation with the Burgers vector $1/6\langle 112\rangle$ parallel to the interface is present for each {111} plane inbetween the two variants. Within the viewing direction used for HRTEM imaging the two twinning variants can be overlapping, giving a typical intensity modulation on top of the HRTEM image as can be observed for the left part of the central twin lamella shown in Fig. 3(a). This effect was also shown and analyzed in more detail for HoH_2.[9] This frequent observation indicates that the boundary between two twin variants is not always the {111} that is parallel to the interface plane.

A crystallographic orientation of YH_2 deviating from the ones previously shown is frequently observed in the cross-sectional TEM samples. In Fig. 4, such a deviating orientation region is shown. However, it is of course not unambiguous to ascribe this deviating orientation to the structure of one of the ridges of the triangular network. Fortunately, the undamaged surface structure of one ridge in cross section is observed as depicted in Fig. 5(a), which corresponds very well (height, asymmetry) with the structure expected from the atomic force microscopy (AFM) observations.[8] Also, the distance between the regions containing the deviating crystallographic orientation in the cross-sectional TEM sample agrees well with the typical distance of about 2 μm between the ridges as observed by AFM for a 500 nm thick YH_x film. Furthermore, additional XRD studies indicate that only two basic orientations are present in the β and γ films, i.e., the domains and ridges. Finally, plan-view TEM observations indeed show that the triangular network of ridges is composed of this single deviating crystallographic orientation.

In comparison with the YH_2 domains the orientation of one of the YH_2 ridges consists of a rotation of about $\pm 19.5°$ or $\pm 90°$ along a $\langle 110\rangle$ direction parallel to the length of the ridge along the surface. For the fcc-type YH_2 no distinction between the two angles can be made, but this ambiguity is lifted if the orientation of the ridges in the hexagonal Y or $YH_{3-\delta}$ is known. The plan-view sample on CaF_2, containing Y ridges and domains clearly showed that the angle between the close-packed (0002) planes of the ridges and domains is $\pm 90°$ and not $\pm 19.5°$. Careful analysis showed that the angle is in fact deviating about 5° from the 90° angle. In plan view the $[0001]$ zone axis of the Y domains is not parallel to the $[01\bar{1}0]$ axis of the Y ridges as would be the case for a 90° angle, but these zone axes have a mutual tilt of about 5° around their common $\langle \bar{2}110\rangle$ axis, which is in plane along the length of the ridges. Also in the cross-sectional HRTEM images of YH_2 it can be observed that the angle

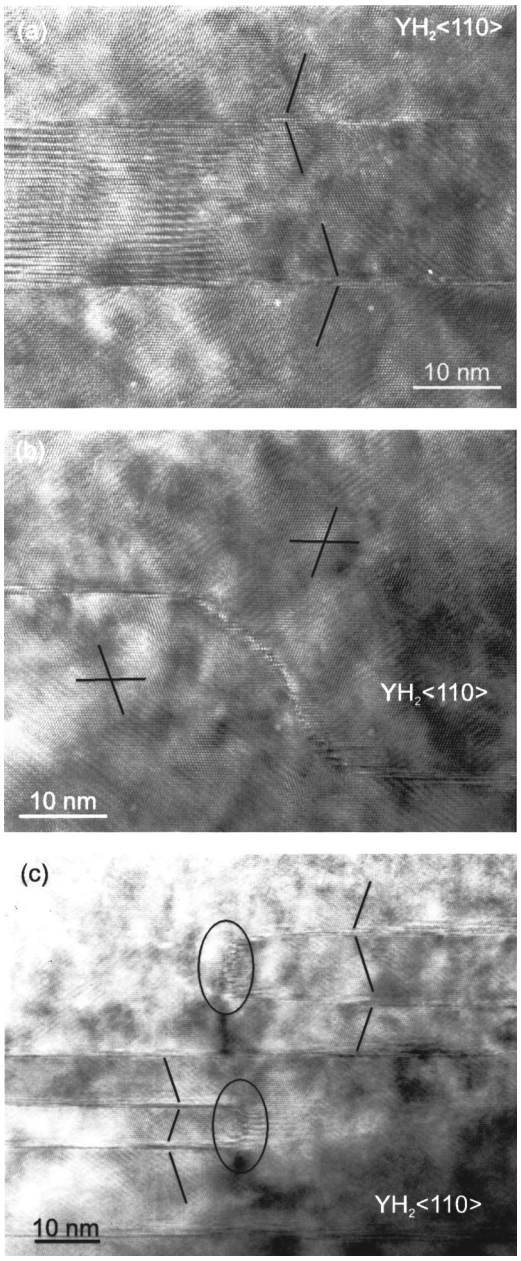

FIG. 3. Cross-sectional HRTEM images showing $\Sigma 3\{111\}$ twin boundaries parallel to the film/substrate interface in the (500 nm high) YH_2 domains. (a) Within the viewing direction used for HRTEM imaging two twinning variants overlap giving a typical intensity modulation on top of the HRTEM image as can be observed in the left part of the central twin lamella. (b) A superledge is present on the twin boundaries with a height parallel to the substrate/film interface normal. (c) Twin lamellae as bounded by two $\Sigma 3\{111\}$ boundaries ''end'' abruptly; the ends are encircled.

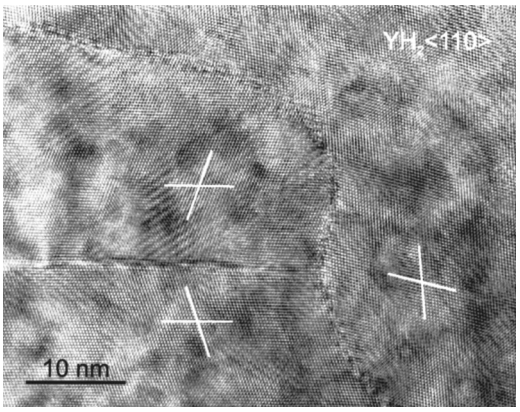

FIG. 4. Cross-sectional HRTEM image showing a crystallographic orientation of YH_2 deviating from the one of the domains; a boundary between a domain region containing a regular twin parallel to the substrate/film interface and this deviating-orientation region is shown.

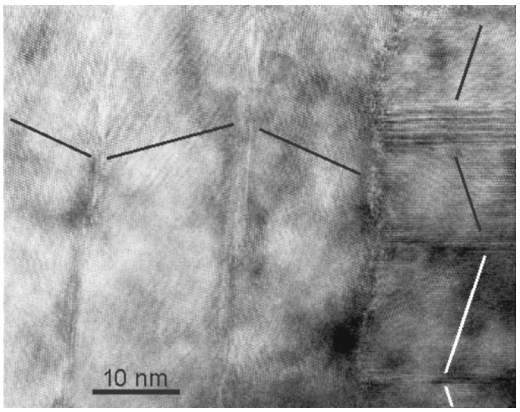

FIG. 6. Cross-sectional HRTEM image showing vertical $\Sigma 3\{111\}$ twin boundaries in a YH_2 ridge adjacent to an YH_2 domain containing horizontal $\Sigma 3\{111\}$ twin boundaries. Note the 95° angle between the twin boundaries of the ridge and the domain; this angle agrees with $(10\bar{1}2)$ twinning in the original Y.

always deviates slightly from 90° (cf. Fig. 4). In contrast to α and β, we were not able to analyze γ with TEM, but using XRD it turned out that the angle is, apart from the slight deviation, always $\pm 19.5°$ and *not* $\pm 90°$. Figure 5(b) shows an overview of the ridge depicted in Fig. 5(a). The ridge spans almost the entire 500 nm thickness of the YH_2 layer and runs roughly parallel to the interface normal. The ridge shown in Fig. 5 consists of two parts that are $\Sigma 3$ twin variants. However, in contrast to the domains where the twin boundary between the variants has the tendency to be parallel to the substrate/film interface, for the ridges it has the tendency to be nearly parallel to the interface normal and runs parallel to the ridge length in the triangular network (i.e., along the $\langle 110\rangle$ YH_2 viewing direction in the cross-section sample). The twin boundary of the ridge in Fig. 5 as well as the boundaries between the ridge and the two neighboring domains is rather wavy. It seems that after the first α to β transition, these three boundaries are relatively flat. However, due to the subsequent reversible β to γ transitions, curved and distorted interfaces have developed. An example of sharp, flat, and edge-on observed $\Sigma 3\{111\}$ twin boundaries in a ridge is shown in Fig. 6. Note in Fig. 6 the general trend that twin boundaries in the ridge are not exactly vertical, but are consistently about 5° off.

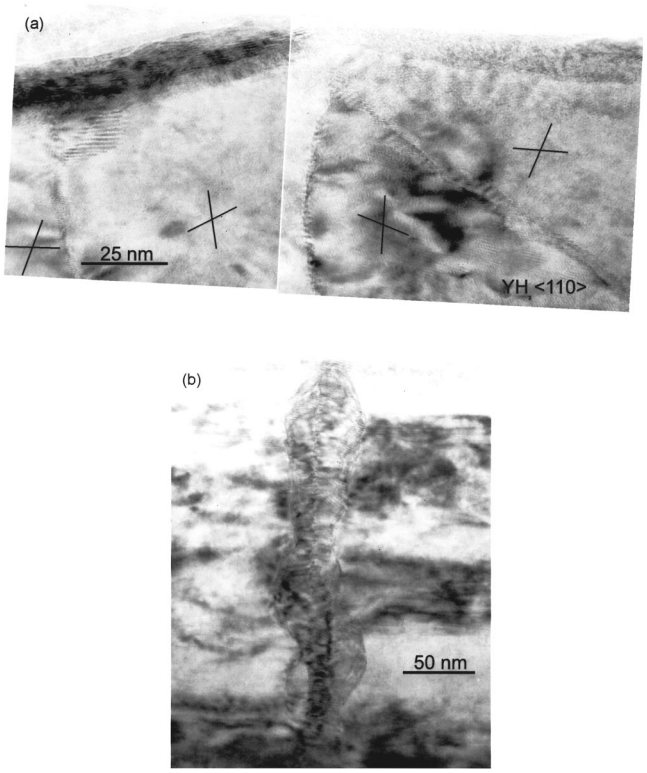

FIG. 5. (a) Cross-sectional HRTEM image showing the undamaged surface structure of a YH_2 ridge. Compared to the orientation of the domains the one of the ridge consists of a roughly $\pm 19.5°$ or $\pm 90°$ rotation along a $\langle 110\rangle$ direction parallel to the length of the ridge along the surface (viewing direction). (b) An overview image of the ridge depicted in (a) is shown. The ridge spans almost the entire 500 nm thickness of the YH_2 layer and runs roughly parallel to the interface normal. The ridge shown consists of two parts that are $\Sigma 3$ twin variants. The twin boundary between the variants has the tendency to be almost parallel to the interface normal (5° off) and runs parallel to the ridge length.

In the plan-view sample on the CaF_2 substrate, regions containing Y domains and ridges are present next to regions containing YH_2 domains and ridges. The selected area electron diffraction (SAED) patterns of the Y domains and one of the three possible orientations (i.e., they differ by rotations of 120° along the viewing direction) of the Y ridges as obtained in plan view are shown in Figs. 7(a) and 7(b). To arrive from the [0001] zone axis of the domain in the $\langle 01\bar{1}0\rangle$ axis of the neighboring ridge a rotation of about 5° is needed around their common $\langle \bar{2}110\rangle$ that is parallel to the ridge length. After the transformation to YH_2 these two Y zone axes for the domains and ridges become $\langle 111\rangle$ and $\langle 11\bar{2}\rangle$, respectively, and the corresponding SAED patterns are shown in Figs. 7(c) and 7(d). Note that the four SAED patterns in Fig. 7 have the same scaling and the correct mutual orientation as they were all obtained from a single epitaxial layer.

In cross section a single $\Sigma 3\{111\}$ twin boundary in each YH_2 ridge is usually observed, but in plan view multiple vertical twin boundaries within a single ridge are also observed (see Fig. 8). The edge-on twin boundaries in the YH_2 ridges cannot be detected when viewing along $\langle 112\rangle$, because

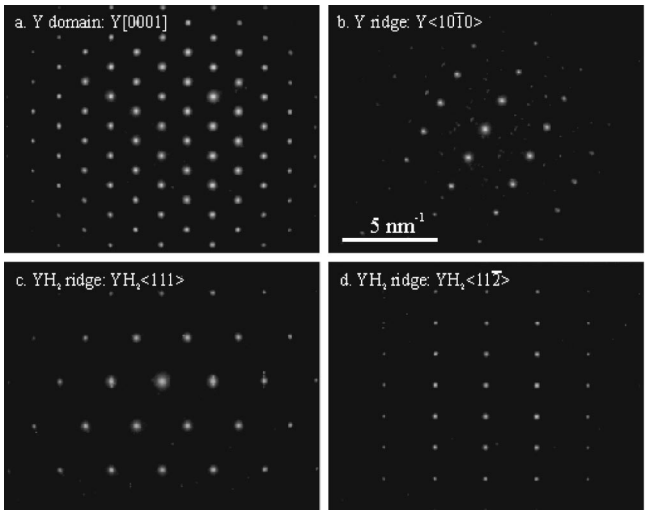

FIG. 7. Representative SAED patterns recorded in plan view for (a) the Y domains, (b) the Y ridges, (c) the YH_2 domains, and (d) the YH_2 ridges. To arrive from the [0001] or $\langle 111\rangle$ zone axis of the domains in the $\langle 01\bar{1}0\rangle$ or $\langle 11\bar{2}\rangle$ axis of the neighboring ridges a rotation of about 5° is needed around their common $\langle \bar{2}110\rangle$ or $\langle 1\bar{1}0\rangle$ that is parallel to the ridge length. Note that the four SAED patterns have the same scaling and the correct mutual orientation as they were obtained from a single epitaxial layer on a CaF_2 substrate.

the crystal orientations on both sides of the boundary are identical for this viewing direction. Instead tilting the sample over 30° to view along a $\langle 110\rangle$ instead of a $\langle 112\rangle$ ridge direction, keeping the $\{111\}$ planes of only one of the three different ridge types edge-on, reveals possible twins in this ridge type. So, Fig. 8 is recorded for viewing along a $\langle 110\rangle$ ridge direction making an angle of 30° with the surface normal. White arrows indicate traces of twin boundaries.

Although only a single crystallographic orientation relation (OR) holds between the ridges and the domains, two types of inclinations of the ridges with respect to the surface normal occur. The ridges run parallel to one of the three in-plane $\langle 110\rangle YH_2$ domain directions (i.e., $\langle 11\bar{2}0\rangle$ domain directions for α and γ). In one case the ridge crosses the film parallel to the substrate/film interface normal and in the other case it is inclined roughly over $45° \pm 5°$. An exact angle cannot be determined, because the interface between the ridge and the domain is very wavy (cf. Fig. 4), even on a magnified scale.

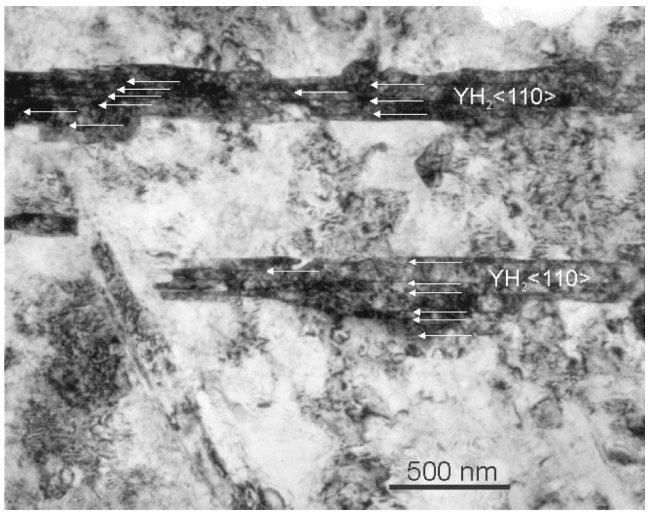

FIG. 8. Plan-view HRTEM image showing YH_2 ridges viewed along their $\langle 110\rangle$ direction making an angle of 30° with the surface normal for a sample grown on a CaF_2 substrate. Note that due to the 30° tilting only one of the three different ridge orientations of the triangular network, showing strong diffraction contrast, remains edge on. Traces of twin boundaries within these ridges are indicated by white arrows.

IV. DISCUSSION

A. Ridge formation

The orientation of the Y ridges compared to the domains as observed by SAED, i.e., a 95° rotation around their common $\langle 11\bar{2}0\rangle$ axis that is parallel to the length of the ridges, is substantial evidence that the ridges are a result of $(10\bar{1}2)$ twinning. This is a very common (deformation) twinning mechanism found in hcp crystals;[12–15] From AFM observations we know that the ridges have an asymmetric surface structure. All ridges appeared to be bounded by a steep and a shallow facet. From the fact that the steep facet ridge makes an average angle of $5.8° \pm 0.2°$ with the surface we already concluded that $(10\bar{1}2)$ twinning had occurred.[8] Although a 95° rotation of the crystal occurs during twinning, the observed shear involved in $(10\bar{1}2)$ twinning is peculiarly small.[11–14] This type of twinning thus experiences relatively little hinder from a constraint from the surrounding that opposes shape changes.

Dislocation mechanisms that explain the observed phenomena of $(10\bar{1}2)$ twinning in hcp have been elaborated on in detail.[12,13,16,17] Generally they are based on a ratchet–pole mechanism, where the starting dislocation has a Burgers vector [0001] that splits up in a sessile pole dislocation around which a glissile dislocation with Burgers vector $\alpha\langle 01\bar{1}1\rangle$ winds [where α depends on the c/a ratio and is relatively small ($\sim 1/12$)]. This type of mechanism is likely to occur because it explains the observed small shear connected to the large crystal reorientation. In Fig. 9 the twinning in the Y film is schematically depicted for the ridges running roughly 45° through the film. This angle is in fact initially probably 47.8°, because then the boundaries between the twin and the domain would be parallel to $(10\bar{1}2)$. In Figs. 10(a) and 10(b) the twinning in the Y film is schematically depicted for ridges that cross the film transversally. During twinning the horizontal (0002) is 5.6° rotated and transformed into $(10\bar{1}0)$ and the vertical prismatic plane is rotated 5.6° and transformed into the basal plane, giving the overall effect that the crystal is rotated 95.6°. The relative steep surface facet of the ridge is thus in all cases $(10\bar{1}0)$, making an angle of 5.6° with the surface in agreement with the original determined angle based on AFM analysis[8] [although the surface facet was at that time indexed erroneously as $(1\bar{1}02)$].

The slip during twinning is less constrained by the neighboring Y in the case of Fig. 9 than in the case of Fig. 10. However, because it is likely that the twins initiate on dislocations, the orientation of these dislocations will affect

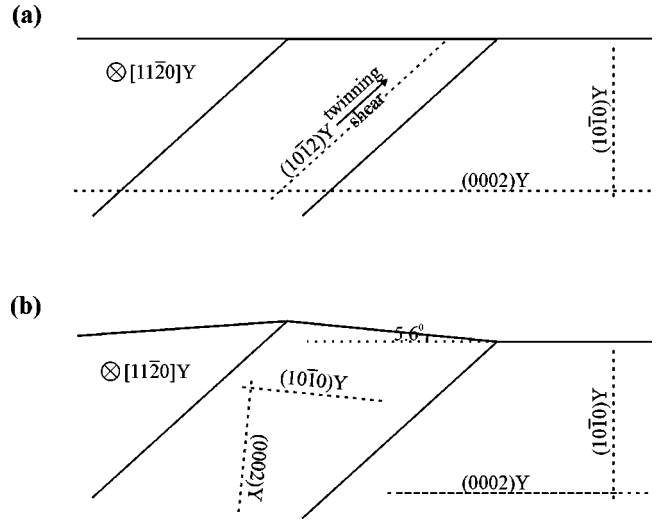

FIG. 9. Schematic representation of $(10\bar{1}2)$ twinning in Y corresponding to a 5.6° shear where the boundaries between the twin and the domains are parallel to $(10\bar{1}2)$.

the orientation of the twin. In the case of an isotropic system a ratchet–pole mechanism would result in a transformed region around the central dislocation that is cylindrical. In the present system strong anisotropy in strains develop during twinning. It causes a clear preference for growth of the transformed region in the thin plate in the unstrained $\langle 11\bar{2}0\rangle$ Y direction that is perpendicular to the shear direction, i.e., parallel to the viewing direction of Figs. 9 and 10. This explains why the ridges are thin long plates. Furthermore, with plan-view TEM it can be observed that many ridges consist of elongated segments in a chain (cf. Fig. 8). These observations are in agreement with a mechanism based on local nucleation of twins, e.g., based on a ratchet–pole mechanism.

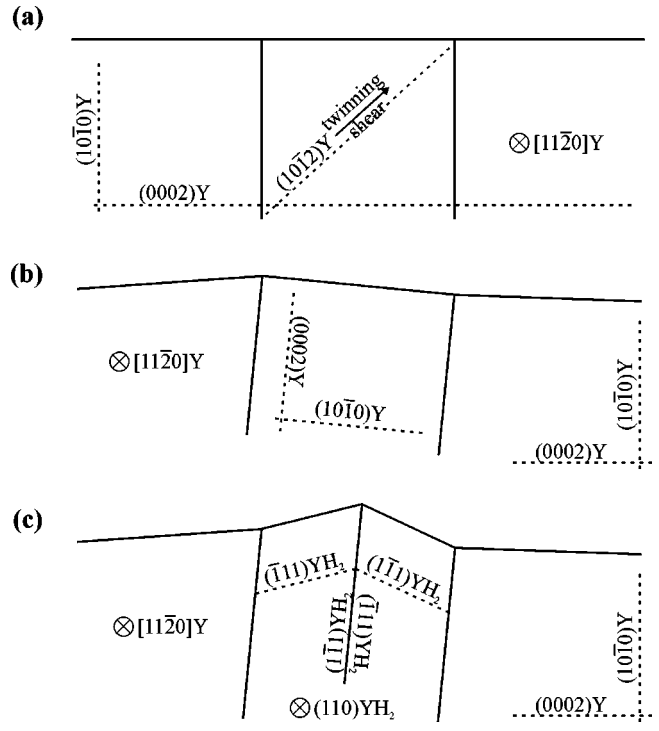

FIG. 10. Schematic representation of $(10\bar{1}2)$ twinning in Y where the boundaries between the twins and the domains are initially parallel to $(10\bar{1}0)$ and the Y during twinning is rotated 5.6°.

During the intake of hydrogen Y already expands in the α phase.[7] Perpendicular to the free surface the expansion is unconstrained, but the in-plane expansion is hindered by the (rigid) substrate and thus impedes the intake of H. It is likely that twinning is initiated by the in-plane expansion of Y during H loading. The fact that in the as-deposited Y film on CaF_2 ridges have also developed is probably also due the presence of compressive stresses,[7] which arise because during cooling from the deposition temperature CaF_2 contracts more than the Y film. To release the strains twinning occurs because the twin pushes material out of the film. The horizontal (0002) plane is, apart from the 5.6° shear rotation, replaced by the $(10\bar{1}0)$ that has a 10.3% larger d spacing. Therefore, an expansion perpendicular to the free surface occurs. On the other hand, the vertical prismatic plane is replaced by the basal plane corresponding to an in-plane contraction of 9.4%. The twin thus locally relaxes the in-plane strains such that other twins only have to develop beyond a typical distance. In this way a ridge network is formed with a typical distance that scales with the thickness of the Y film[8] in agreement with experimental observations. The in-plane contraction of the twins paves the way for the subsequent transformation of the Y domains into YH_2, which is associated with an in-plane expansion of 1.0%.

The network of ridges on epitaxial YH_x films on CaF_2 is already fully developed after the initial α-Y to β-YH_2 transformation, whereas on epitaxial YH_x films on sapphire ridges still develop after the subsequent transformation to γ-YH_3. In both cases the same $(10\bar{1}2)$ twinning mechanism is at the origin of the ridges (either in hexagonal α or γ), but the onset of twinning is earlier on CaF_2 than on α-Al_2O_3, because compressive stresses in the as-deposited films are present with the former[7] and absent with the latter substrate,[9] and because the in-plane thermal expansion of Y and α-Al_2O_3 is much better matched.

The transformation from Y to YH_2 is, from a crystallographic viewpoint, analogous to the Ti to TiH_2 transformation. From the extensive literature on Ti/TiH_2[18–22] it is well known that TiH_2 plates precipitate preferably on prismatic planes of Ti and for viewing along the [0001]Ti direction a triangular network of precipitates develops in exactly the same manner as the network that develops during the Y to YH_2 transformation. The common orientation relation found between TiH_2 and Ti is $\{110\}//\{01\bar{1}0\}$,$\langle 001\rangle//[0001]$,[18–22] however two other ORs are also reported, one of which is $\{111\}//\{01\bar{1}0\}$,$\langle 11\bar{2}\rangle//[0001]$.[18,20] This latter OR is identical to the one found in the present YH_2 films if the domains are still considered to be in the hexagonal Y state. It is generally assumed that the TiH_2 precipitates nucleate and grow fast by a terrace-ledge-kink mechanism.[22,23] Although, all the observations in the present work on the triangular network that forms in the YH_x films can be explained by $(10\bar{1}2)$ twinning, it cannot be excluded that during the α-β transfor-

mation YH_2 precipitates first nucleate on prismatic Y planes before the domains transform.

B. The hcp–fcc transformation

The transformation within the domains, both the initial α-β as well as the reversible β-γ, shows clear classical signs of the hcp–fcc transformation involving the glide of Shockley partial dislocations on each second close-packed plane.[24] If these partial dislocations have Burgers vectors equally and alternately divided over the three possible close-packed directions in the set of horizontal close-packed planes the shear would not occur and the macroscopic shape change would be equal to zero.[24–27] However, the TEM observations show that the Burgers vectors are predominantly of one particular type. These observations indicate that the partials did not self-nucleate sequentially[28] because then the constraint to prevent shear and shape changes would have caused the equal and alternate division of the Burgers vectors over the three possible close-packed directions. Consequently, a transformation shear is unavoidable. Still, to avoid the macroscopic shape changes, which is important because the domains are bound by unmovable ridges, twinning is introduced with horizontal $\Sigma 3\{111\}$ twin boundaries as schematically shown in Fig. 11. Twinning will only occur if the total thickness of the Y film is sufficient, e.g., starting with a film thickness of about 80 nm.

In the ridges the transformation from α to β proceeds analogously to the transition in the domains with slip of Shockley partial dislocations on each second basal plane. However, a crucial difference is that the basal plane is horizontal in the domains and more or less vertical in the ridges. At the ridge/domain boundary the shear due to the glide of Shockley partial dislocations is opposed. For the ridges crossing the film transversally an obvious result of the α-β transition leads to a configuration as schematically depicted in Fig. 10(c) with at least one vertical twin boundary in the ridge in agreement with the experimental findings. Depending on the thickness of the ridges more vertical twin boundaries can be introduced to reduce the shape changes at the interface with the substrate, because clamping by the substrate will retain shape changes.

As shown in Sec. II many (large) steps and ledges are present on the twin boundaries in β-YH_2 [Fig. 3(b)] and twin lamellae can also stop abruptly [Fig. 3(c)] giving rise to the presence of Shockley partial dislocations on each successive close-packed plane at all these locations. These Shockley partial dislocations are excellent sources for the β–γ transformation. Like unzipping, one half of the Shockley dislocations on the ''even'' close-packed planes can move to one side and the other half on the ''odd'' planes moves to the other side leaving a transformed region inbetween in their wake. This process greatly facilitates the transformation, because the nucleation of Shockley dislocations can be omitted. Shockley partial dislocations can move up to the ridges and may be absorbed in the ridge/domain interface. During the reverse γ–β transformation the Shockley dislocations can be released again and they can move into the domains establishing the transformation. In this manner the reversible switching of the mirror can operate efficiently.

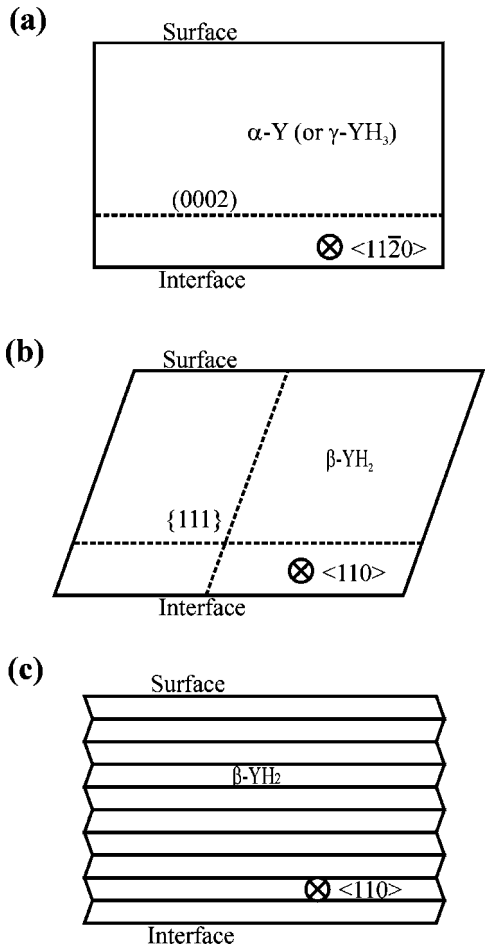

FIG. 11. Schematic representation of the shape changes associated with the formation of a YH_2 domain out of Y or YH_3: (a) an initially rectangular Y or YH_3 block clamped by the substrate as viewed along $\langle 11\bar{2}0\rangle$; (b) the shape change (transformation shear) if YH_2 is formed by the slip of Shockley partial dislocations, all having the same Burgers vector and slip direction, on each second basal plane of the Y or YH_3; (c) the shape change if YH_2 is internally twinned is possible by slip of Shockley partial dislocations with identical Burgers vectors but with slip in alternating lamellae in opposite directions.

Once arrived from the hcp α phase in the fcc β phase two sets of close-packed planes become available as slip system for the Shockley partial dislocations. In the domains one set is horizontal (parallel to the interface with the substrate) and the other set 70.5° is inclined. In the ridges one set is (neglecting the 5.6° rotation due to twinning) 19.5° inclined and the other 90°. In principle it is possible that during the subsequent β–γ transformation the single crystallographic orientation relation between domains or ridges and the substrate become double. XRD pole figures clearly demonstrate that this process does not occur. During the reversible β–γ transformation the c axis of γ in the domains always remains perpendicular to the free surface and is inclined over 19.5° in the ridges. This strong preference for keeping the c axis as perpendicular as possible to the free surface can be understood, because a large expansion along the c axis of 10.6%

occurs, whereas the expansion for directions within the basal plane is negligibly small.

C. The independent switching of domains and ridges

We observed pixel-like switching of the domains in epitaxial YH_x films.[8] Starting from a film in the β-YH_2 phase, upon loading the domains first transform individually into γ-$YH_{3-\delta}$, whereas the ridges still remain β-YH_2. The ridges finally switch collectively. During the reverse transformation the ridges first transform back collectively to β, whereas the domains return later individually. The delayed transformation of the ridges from β to γ can be explained based on the results from the TEM analysis, i.e., the expansion of 10.6% for the domains is perpendicular to the free surface and for the ridges inclined 19.5°. The in-plane component of the expansion of the ridges hampers their transformation. Furthermore, the stress introduced with their transformation also destabilizes the γ phase in the ridges and consequently they tend to transform sooner back to β. The asymmetry of the ridges affects the individual switching kinetics of the neighboring domains.[29] If domains are bordered on all sides by the steep side of the ridges they switch later. On the other hand if they are bordered on all sides by the flatter side of the ridges, they switch earlier. More details on this behavior are given in Ref. 29.

The final issue to be addressed is the mechanism by which the ridges and domains are able to cope with their huge differences in expansion when they do not switch simultaneously. During the pixel switching the domains expand 10.6% perpendicular to the surface, whereas the ridges remain untransformed. These expansion differences can only be accommodated plastically and again glide of dislocations must be involved. Figure 12 demonstrates a mechanism starting with an fcc wedge-shaped ridge (width linearly increasing from zero at the film/substrate interface) containing a vertical twin boundary in the center that can accommodate *exactly* the required vertical expansion at all heights in the neighboring domain. Still the domains on both sides of the ridge can switch independently. Moreover, the $\beta-\gamma$ transition can be accommodated not only once, but approximately over numerous cycles (see Fig. 12). The approximation involved implies that the shape changes associated with the fcc–hcp transitions (involving shear) are neglected; only the expansions of the lattices due to intake of hydrogen are considered. For a 10.6% expansion of the domains the semiangle of the wedge shape is 8.5° ($\arctan(0.053\tan(70.5°))$). The width of the wedge at the top of a 500 nm film is 150 nm. In Fig. 12(b) the domains neighboring the ridge have expanded 10.6% due to the $\beta-\gamma$ transition and the ridge has responded by the glide of Shockley partial dislocations on each vertical close-packed plane, but is still in the β phase. Then the ridge transforms from β to γ by: (1) a reversed glide of the Shockley partial dislocations on each vertical plane followed by (2) the glide of Shockley partial dislocations on each second 19.5° inclined close-packed plane. Note that (2) already can start when (1) has proceeded only a short distance, e.g., from the bottom up in the ridge. In this way processes (1) and (2) will cooperetive closely. The final result with both the ridges and domains in the γ phase is shown in Fig. 12(c). For the reverse transformation of the ridges and domains the reverse processes hold, i.e., from Fig. 12(c) via 12(b) back to 12(a). The final situation where both the ridges and domains have returned to the β phase is displayed in Fig. 12(a). The system is then ready for another cycle. In the mechanism depicted in Fig. 12 the vertical twin boundary acts as a hinge and both sides of the hinge can rotate independently. The same mechanism still works if the ridge consists of more than one vertical twin boundary. Only the two outer arms of the hinge are important. Of course this mechanism is a simplification of reality. The exact wedge shape with the correct semiangle will not occur. However, the width of a vertical twin lamella observed in the ridges is on average about 40 nm. This would mean that the arm of the hinge is still correct near the center of the film with a thickness of 500 nm. Near the bottom and

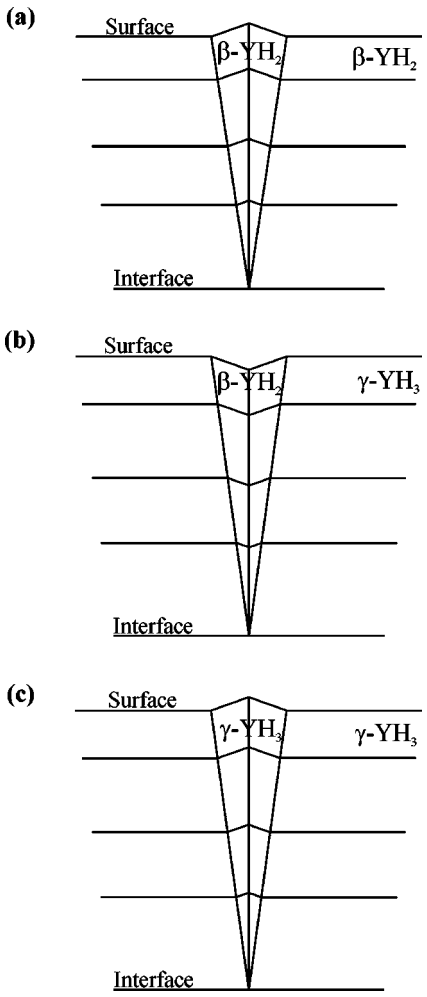

FIG. 12. Schematic representation of the reversible independent switching of the domains and ridges between YH_2 and YH_3 with the ridges acting as hinges: (a) a wedge-shaped YH_2 ridge (wedge angle 17°) containing a vertical $\Sigma3\{111\}$ twin boundary is present inbetween YH_2 domains; viewing direction $\langle 110\rangle$; (b) the domains have transformed into YH_3, expanded 10.6% perpendicular to the free surface, and the YH_2 ridge has *exactly* followed this expansion by changing the configuration of the twin; (c) the ridge has finally also been transformed into YH_3 by again changing the configuration of the twin followed by the slip of Shockley partial dislocations on each second most horizontal close-packed plane in the YH_2. The reverse switching from YH_3 to YH_2 follows the reverse route from 10*c* through *b* to *a*.

top the expansion of the domain will not be accommodated correctly, but still the largest portion of the expansion difference between ridge and domain is accounted for. Second, the shape changes due to the change in crystallography (excluding expansions) may spoil this mechanism. However, as depicted in Fig. 11 most of the macroscopic shape changes in the domains or ridges vanish due to the horizontal or vertical twin boundaries, respectively.

The total switching behavior of the epitaxial YH_x switchable mirror is an intricate interplay of mechanisms like the one depicted in Figs. 11(a) and 11(c), which account for the change in crystallography and the one displayed in Fig. 12 that accounts for the difference in lattice expansions due to the hydrogen uptake. All steps of the reversible transformation between β and γ proceed by the movement of Shockley partial dislocations on close-packed planes. Although switching of the mirror relies upon processes that are quite reversible, in the end the total process will suffer from the gradual buildup of irreversible distortions. See, for instance, Fig. 5(b), where the ridge with initial flat vertical boundaries has become clearly distorted after switching of the mirror.

V. CONCLUSIONS

A detailed understanding of the mechanisms of the phase transformations in epitaxial switchable mirrors is obtained using HRTEM. It is shown that prior to the α-Y to β-YH_2 transformation a triangular network develops due to $(10\bar{1}2)$ twinning. Twinning occurs in α-Y to relax the compressive strain buildup due to the intake of H. The basal plane that is originally parallel to the film/substrate interface rotates by twinning over 5.6° and transforms into a prismatic plane. In the same way the vertical prismatic plane is replaced by the basal plane and the overall rotation of the crystal is 95.6°.

The transformations among the hexagonal (α-Y and γ-$YH_{3-\delta}$) and fcc (β-YH_2) phases proceed by the glide of Shockley partial dislocations on each second basal plane. To prevent macroscopic shape changes in the domains, a larger number of horizontal $\Sigma 3\{111\}$ twin boundaries develop within the YH_2. The reversible β–γ transformation is greatly facilitated by the numerous Shockley partial dislocations present at the boundaries between the two twin variants in the domains and their presence avoids the need for nucleating these partials. After the initial α–β transformation nearly vertical twin boundaries arise in the ridges.

On top of the shape changes intrinsic to the phase transformations considerable anisotropic expansions of the lattices occur due to the intake of hydrogen. The dominant expansion occurs along the *c* axes of the hexagonal α-Y and γ-$YH_{3-\delta}$ phases and during the β–γ transformations both the domains and the ridges choose to keep this *c* axis as perpendicular as possible to the free surface. With respect to the domains a delayed β–γ transformation is observed in the ridges, which can be understood, because the in-plane expansion of the ridges hampers their transformation. On the other hand, the domains expand 10.6% perpendicular to the surface. It is rationalized that the vertical twin boundaries in the ridges act as hinges, allowing for the largest differences in expansion between the ridges and domains to be absorbed. Our analysis shows the feasibility of operating twinned epitaxial switchable mirrors over many cycles.

ACKNOWLEDGMENTS

U. Nieborg is gratefully acknowledged for preparation of all TEM specimens. A. Remhof is thanked for discussions.

[1] J. N. Huiberts, R. Griessen, J. H. Rector, R. J. Wijngaarden, J. P. Dekker, D. G. de Groot, and N. J. Koeman, Nature (London) **380**, 231 (1996).
[2] P. J. Kelly, J. P. Dekker, and R. Strumpf, Phys. Rev. Lett. **78**, 1315 (1997).
[3] K. K. Ng, F. C. Zhang, V. I. Anisomov, and T. M. Rice, Phys. Rev. B **59**, 5398 (1999).
[4] R. Eder, H. A. Pen, and G. A. Sawatzky, Phys. Rev. B **56**, 10115 (1997).
[5] F. J. A. den Broeder *et al.*, Nature (London) **394**, 656 (1998).
[6] R. Armitage, M. Rubin, T. Richardson, N. O'Brien, and Y. Chen, Appl. Phys. Lett. **75**, 1863 (1999).
[7] D. G. Nagengast, J. W. J. Kerssemakers, A. T. M. van Gogh, B. Dam, and R. Griessen, Appl. Phys. Lett. **75**, 1724 (1999).
[8] J. W. J. Kerssemakers, S. J. van der Molen, N. J. Koeman, R. Günther, and R. Griessen, Nature (London) **406**, 489 (2000).
[9] E. J. Grier, O. Kolosov, A. K. Petford-Long, R. C. C. Ward, M. R. Wells, and B. Hjörvarsson, J. Phys. D **33**, 894 (2000).
[10] A. Pundt, M. Getzlaff, M. Bode, R. Kirchheim, and R. Wiesendanger, Phys. Rev. B **61**, 9964 (2000).
[11] A. Remhof, G. Song, Ch. Sutter, A. Schreyer, R. Siebrecht, and H. Zabel, Phys. Rev. B **59**, 6689 (1999).
[12] N. Thompson and D. J. Milliard, Philos. Mag. **43**, 422 (1952).
[13] D. G. Westlake, Acta Metall. **9**, 327 (1961).
[14] M. V. Klassen-Neklyudova, *Mechanical Twinning of Crystals* (Consultants Bureau, New York, 1964), p. 167.
[15] H. S. Rosenbaum, in *Deformation Twinning*, edited by R. E. Reed-Hill, J. P. Hirth, and H. C. Rogers (Gordon and Breach Science, New York, 1963), p. 43.
[16] D. G. Westlake, in *Deformation Twinning*, edited by R. E. Reed-Hill, J. P. Hirth, and H. C. Rogers (Gordon and Breach Science, New York, 1963), p. 33.
[17] J. P. Hirth and J. Lothe, *Theory of Dislocations* (Wiley, New York, 1982), pp. 818–825.
[18] J. D. Boyd, Quart. Trans. Am. Soc. Metals **62**, 977 (1969).
[19] J. D. Boyd, *The Science, Technology and Applications of Titanium*, edited by R. I. Jaffee and N. E. Promise (Pergamon, Oxford, 1970), p. 545.
[20] J. W. Edington, *Practical Electron Microscopy in Materials Science; Monograph Four* (The Macmillan Press, London, 1976), p. 56.
[21] H. Numakura and M. Koiwa, Acta Metall. **32**, 1799 (1984).
[22] A. Bourret, A. Lasalmonie, and S. Naka, Scr. Metall. **20**, 861 (1986).
[23] H. Gleiter, Acta Metall. **17**, 565 (1969); **17**, 853 (1969).
[24] D. A. Porter and K. E. Easterling, *Phase Transformations in Metals and Alloys* (Van Nostrand Reinhold, New York, 1981), pp. 164–169.
[25] J. M. Howe, U. Dahmen, and R. Gronsky, Philos. Mag. A **56**, 31 (1987).
[26] N. Prabhu and J. M. Howe, Scr. Metall. **22**, 425 (1988).
[27] T. Furuhara and T. Maki, Scr. Mater. **929**, 34 (1996).
[28] J. A. Hren and G. Thomas, Trans. AIME **308**, 227 (1963).
[29] J. W. J. Kerssemakers, B. Dam, and R. Griessen (unpublished).